Classical molecular dynamical simulations of high pressure behavior of alpha cristobalite (SiO_2)

2007 J. Phys.: Condens. Matter 19 456201

(http://iopscience.iop.org/0953-8984/19/45/456201)

IOP PUBLISHING JOURNAL OF PHYSICS: CONDENSED MATTER

J. Phys.: Condens. Matter **19** (2007) 456201 (15pp) doi:10.1088/0953-8984/19/45/456201

Classical molecular dynamical simulations of high pressure behavior of alpha cristobalite (SiO_2)

Nandini Garg[1] **and Surinder M Sharma**

High Pressure Physics Division, Bhabha Atomic Research Center, Trombay, Mumbai 400085, India

E-mail: nandini@magnum.barc.ernet.in

Received 1 June 2007, in final form 15 August 2007
Published 11 October 2007
Online at stacks.iop.org/JPhysCM/19/456201

Abstract

Static and dynamic high pressure experiments reveal that the behavior of α-cristobalite (SiO_2) depends on the rate and the nature of stress loading. To understand this behavior we have carried out extensive molecular dynamics simulations. The response to rapid and simultaneous increase of the pressures and temperatures to the expected Hugoniot values was calculated. These simulations along the simulated Hugoniot path revealed that alpha cristobalite transforms to a new six coordinated phase beyond 16 GPa, 1410.3 K. We find that between 16 and 18 GPa, even after equilibrating for a very long time, the disorder in the stishovite-like phase persists. On release of pressure, this disordered state is retained, in agreement with the experimental observations. Simulations under slow pressure increase show that the observation of *Cmcm* is sensitive to pressure steps and that stishovite phase arises through the *Cmcm* phase.

(Some figures in this article are in colour only in the electronic version)

1. Introduction

Due to their abundance in the earth's mantle, tectosilicates in general, and silica and its polymorphs in particular, are the most important geological minerals. Also due to their geophysical relevance, their high pressure behavior is of considerable importance. At low pressures, most of these minerals exist in corner linked framework structures and display a typical intrinsic behavior of Si–O linkages. Cristobalite, the mineral of interest in the present study, is a high temperature polymorph of silica and is often found in volcanic rocks. Its idealized structure at high temperatures is cubic (β-phase), which, on lowering the temperature, completely and displacively converts into a tetragonal form (α-phase, also called low cristobalite). Low cristobalite comprises a three dimensional network of corner

[1] Author to whom any correspondence should be addressed.

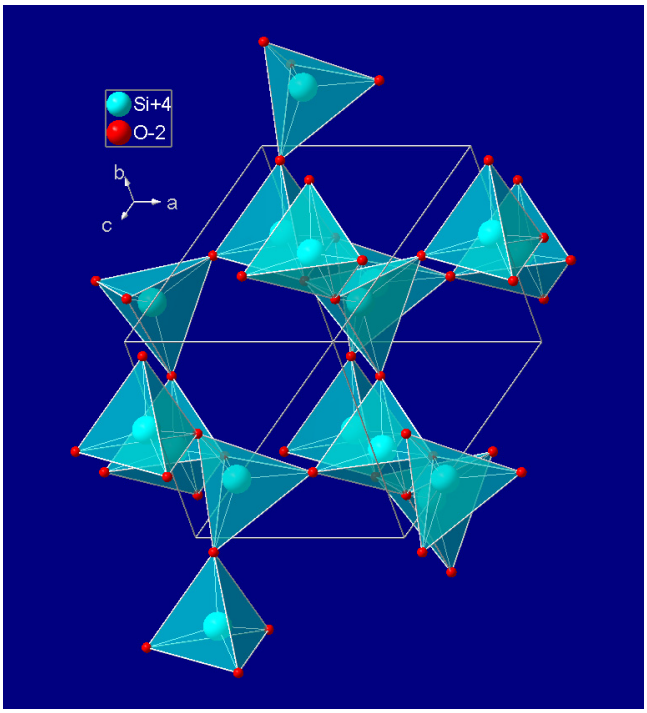

Figure 1. Structure of α-cristobalite perpendicular to the (111) plane.

sharing SiO_4 tetrahedra, and since each oxygen is a bridging atom its structure is a fully polymerized tetrahedral framework (figure 1). As this metastable phase is a descendant of the high temperature phase, its high pressure behavior may also be of relevance, to understand the phases preserved after meteoritic impacts etc. For these reasons, low cristobalite has been investigated, both experimentally as well as theoretically.

High pressure behavior of α cristobalite displays distinct differences when it is subjected to shock [1] and static [2, 3] pressures. Gratz *et al* [1] observed that when powder specimens of α cristobalite were shocked to 28.2 GPa, the recovered samples were almost completely amorphous. However, the specimens shocked to pressures lower than 22.9 GPa retained their original structure[2]. In contrast, under static high pressures, depending on the amount of non-hydrostatic stresses present, low cristobalite displays several crystalline $\rightarrow$ crystalline phase transitions. In a quasi-hydrostatic environment it transforms from alpha to a 'stishovite-like' phase at 18 GPa [4]. However, under non-hydrostatic conditions (without pressure transmitting medium) it first transforms to an intermediate phase [5] (termed X-I) at $\sim$10–15 GPa, which eventually transforms to 'stishovite-like' phase at $\sim$20–30 GPa [4, 5].

The high pressure phase was termed stishovite-like since the additional diffraction line observed by Yamakata *et al* [4] at $d \sim 3.5$ Å could not be indexed with the rutile structure. In addition, broad diffraction peaks of this phase indicate the existence of disorder in this phase. On laser heating, this phase transforms to proper stishovite phase [4]. In addition to the phase transitions mentioned above, some recent Raman [6] and x-ray diffraction [2, 3, 7, 8] studies display the existence of a displacive phase transition to a monoclinic structure at

[2] Though the x-ray diffraction, TEM and SEM studies suggested no amorphization below 22.9 GPa, the Raman spectra of samples shocked to 18.2 and 22.9 GPa indicated broad features.

$\sim$1.5 GPa. However, we must point out that there is an element of irreproducibility in this transformation [4].

Theoretically, the high pressure behavior of α-cristobalite has been investigated by molecular dynamics simulations (MD) [9–13] and total energy calculations [14]. Low pressure transformation to monoclinic phase has been shown to arise via high temperature β-phase [13]. MD calculations of Tsuneyuki et al [9] showed that α-cristobalite transforms to an orthorhombic phase (*Cmcm*) at 16.5 GPa, which further transforms to stishovite at 23 GPa. They had also observed that if $3 \times 3 \times 3$ unit cells were used in the MD macrocell instead of $4 \times 4 \times 3$ unit cells, the *Cmcm* phase[3] was bypassed. Using the pair potentials developed by Van Beest *et al* [15], Tse and Klug [11] showed that α phase transforms directly to stishovite phase at 16 GPa, bypassing the *Cmcm* phase[4]. Recent *ab initio* MD studies of Klug *et al* [16] (using 48 atoms) have shown that under hydrostatic conditions cristobalite transforms via a two step process. First the SiO_4 tetrahedra rotate and then there is a lattice distortion which leads directly to the six coordinated stishovite structure at $\sim$40 GPa. They have also shown that at higher pressures stishovite transforms to a $CaCl_2$ ($P2_1/n$) type structure at 11 Mbar and subsequently to a nine coordinated $P2_1/m$ structure at 14 Mbar. However, neither of these theoretical studies implies a pressure induced amorphization of cristobalite.

To understand the atomic mechanism of some of these structural phase transformations in cristobalite under high pressure we have now again carried out detailed MD simulations. These simulations are likely to be more reliable as we use a large macrocell having an order of magnitude more atoms than used in the earlier MD studies. We have also investigated the variations in crystalline structure, when cristobalite is subjected to pressure (**P**) and temperature (**T**) conditions characteristic of the Hugoniot[5] of the powder sample. Our investigations also help us to understand the atomic rearrangements required for α-phase $\rightarrow$ *Cmcm* $\rightarrow$ stishovite phase transitions.

The present paper has been organized as follows. Section 2 summarizes the essential computational details and **P**, **T**, conditions for which simulations have been carried out. In section 3.1 we present our results which might help the understanding of the results of recovered samples after shock loading. Section 3.2 gives our results of simulations for the hydrostatic pressure conditions. Section 3.3 presents the insight obtained for the understanding of α phase $\rightarrow$ *Cmcm* $\rightarrow$ stishovite phase transitions. Section 4 summarizes conclusions obtained from the present investigations.

2. Computational details

Molecular dynamical simulations (MD) presented here were carried out using a modified [17] Nose–Hoover (N, **P**, **T**) algorithm [18] for variable cell size and shape. These calculations were carried out using the DL POLY package [19] for molecular simulations. Equations of motion were integrated every 2 fs using Verlet's method. The MD cell was considered equilibrated when the fluctuations in temperature, pressure, volume and total energy of the system were less than 0.001%. As mentioned above, a large macrocell was used to minimize the effect of periodic boundary conditions. Most of the simulations were carried out using a macrocell having $8 \times 8 \times 6$ unit cells of α-cristobalite (4608 atoms). For SiO_2 the pair potentials

[3] The *Cmcm* phase is made up of two unit cells of the α phase.

[4] It is interesting to note that Tse and Klug used 216 SiO_2 units in their calculations of the alpha phase in the macrocell. In view of earlier discussions, it follows that they could not have taken an even number of unit cells in the basal plane. Their results appear to prove Tsuneyuki's observations discussed at the beginning of this paragraph.

[5] **P**, **T** along the Hugoniot were calculated using jump conditions with the initial density of the samples as 2.33 gm cm^{-3}, which is the same as in the samples used by Gratz *et al* [1].

Table 1. Simulation pressures and temperatures for rapid and simultaneous increase (representative of shock Hugoniot of [1]).

Shock Hugoniot		
	P (GPa)	**T** (K)
(**a**)	10.0	956.1
(**b**)	13.4	1196.6
(**c**)	16.3	1410.1
(**d**)	18.1	1542.6
(**e**)	19.9	1682.9
(**f**)	20.9	1755.9
(**g**)	22.4	1869.1

of Tsuneyuki *et al* (TTAM) [9, 10] as well as those of van Beest *et al* (BKS) [15] have proven to be equally good for many of the simulations. Most of our calculations were carried out using the BKS potentials [15] except in cases where it is known that the pair potentials of Tsuneyuki *et al* (TTAM) give different results. In those cases, simulations were repeated using TTAM potentials as well. The starting α-cristobalite structure (**P** $=$ 0.1 MPa and **T** $=$ 300 K) was obtained starting from the experimentally known coordinates of this structure [20] and then equilibrating. At each temperature and pressure the system was equilibrated for $\sim$40 ps and the atomic coordinates, volume and pressure of the macrocell were averaged over several thousand time steps. However, at (**P**) and (**T**) where a phase transformation takes place, equilibration was carried out until the thermodynamic quantities converged.

For representing the behavior of shocked samples, simulations were carried at **P** and **T** which correspond to the Hugoniot of porous α-cristobalite as mentioned in section 3.1. These simulations were carried out using the BKS pair potentials. Here we would like to mention that though the simulation methodology for shock propagation in solids is well established [21], in essence these simulations are essentially on single crystals (though, maybe, with some well defined defects). So far no such simulations have been carried out on porous powder samples. As in a single crystal under shock the temperature increase would be negligible compared to that in a porous sample, such a simulation is unlikely to represent the experimental conditions encountered in shocked porous powder. We may also note that since the shock experiments were carried out on porous powders, the deviatoric stresses may not be so vitally important in influencing the experimental results as in a single crystalline sample. Instead, we feel that the high strain rates coupled with **P**, **T** conditions of a shocked porous cristobalite are more likely to be responsible for the experimental results observed by Gratz *et al*. Hence, in our simulations, **T** and **P** were not raised slowly and sequentially as is usually done. Instead the equilibrated phase at ambient conditions was instantaneously subjected to final **T** and **P**. However, dynamically, **P** and **T** approach close to the required values over several tens of time steps and eventual equilibration is a very slow process. Table 1 gives the summary of **P** and **T** conditions at which simulations have been carried out. Also to make a contact with the results of recovered samples after shock loading one must evaluate the effect of residual temperatures on shock release. In the absence of knowledge of these residual temperatures we arbitrarily reduced the **P** and **T** to 0.1 MPa and **T** $=$ 1200, 1000, 500 K, as given in table 2.

To analyze the behavior of α-cristobalite under static pressures, the following simulations were carried out.

(1) Increase of pressure up to 15 GPa in steps of 5 GPa.
(2) Increase of pressure up to 18 GPa in steps of 1 GPa.
(3) Increase of temperature to 1000 and 1996 K after equilibration at 10 GPa.

Table 2. Release of pressure and temperature from some points of table 1 to lower residual temperatures.

Release	
From	To
(a) 18.1 GPa, 1542.6 K	0.1 MPa, 500 K
(b) 19.9 GPa, 1682.9 K	0.1 MPa, 1200 K
(c) 19.9 GPa, 1682.9 K	0.1 MPa, 1000 K
(d) 19.9 GPa, 1682.9 K	0.1 MPa, 500 K
Annealing	
Amorphous phase in step (**a**)	1000 K

We first carried out all these simulations using BKS potentials [15]. As discussed in section 3.1, BKS potentials do not stabilize *Cmcm* phase obtained in the simulations of Tsuneyuki *et al*. Therefore, these calculations under the static pressures were repeated with the TTAM pair potentials [9, 10].

3. Results and discussion

As mentioned in the last section, α-cristobalite phase was generated from the equilibration of the experimentally determined structure. For this the macrocell was equilibrated at 0.1 MPa, 300 K. The equilibrated crystallographic unit cell has somewhat smaller volume (165 Å^3) than the experimentally determined value (170 Å^3). This, as also noted in earlier theoretical studies [10, 11], is due to the smaller Si–O–Si angle in the computed results which leads to a smaller **c**-axis of the unit cell. Figure 2 shows the equilibrated α-phase along [100] and [101] directions. One can discern a small amount of shear in [101] direction when compared to the ideal structure. However, our computed powder x-ray diffraction pattern at 0.1 MPa shows that the magnitude of shear is too small to bring about any observable change in the diffraction pattern.

3.1. Simulations along the calculated shock Hugoniot

As mentioned in section 2, the state equivalent to what is realized under shock is generated by fast increase of pressures and temperatures to the values expected in the experiment. Because experiments were carried out on the powder samples, it is reasonable to treat the material as being under isotropic pressure. In a sense, these simulations represent the effect of rapid and simultaneous increase in mean stress and temperature and thus ignore the effects of the deviatoric stresses, if any. Even in doing so there is no way to ensure that the thermodynamic variables **P** and **T** in the simulations increase in the same manner as in the experiments (i.e. reverberations)[6]. Hence the present results should be taken to represent the gross features of the powder samples subjected to shocks.

Simulations were carried out at a few **P** and **T** listed in table 1. Below point **c** (**P** = 16.3 GPa, **T** = 1410.1 K) the macrocell equilibrates reasonably fast and the crystalline state continues to exist in the α-phase. However, at **c** and **d** (16.3 GPa, 1410.1 K, and 18.1 GPa,

[6] In the recovery capsule of the experiments, the final pressure is achieved through reverberations. Only 50% of the final pressure is achieved with the first shock wave. As we used the single shock jump conditions to simulate **P** and **T**, the temperatures used in the present simulations may be somewhat overestimated.

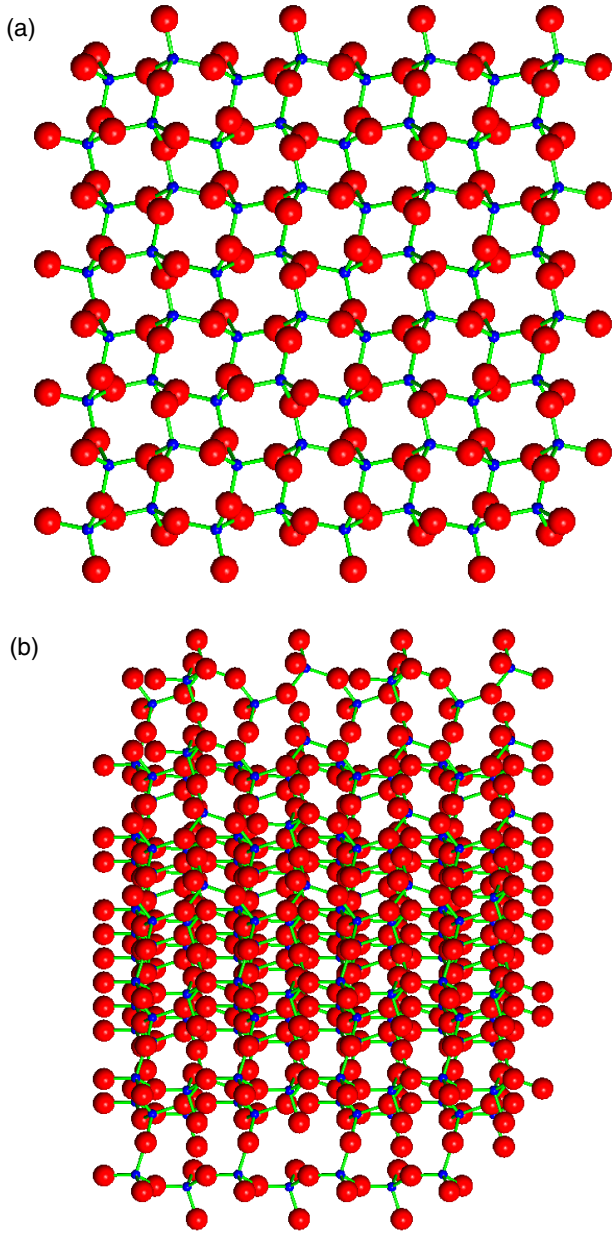

Figure 2. Simulated α-cristobalite structure viewed along (a) the [0 0 1] direction and (b) the [1 0 1] direction, highlighting the existence of a small amount of shear deformation of the cell.

1542.6 K) the α-phase evolves very slowly to the new structure. It took ∼750 ps for the new structure to stabilize. This new structure, as well as all the other equilibrated structures beyond the point **c** in table 1, have six coordination. However, various structures differ from each other in terms of the degree of crystalline order. Also the time taken for the final states to equilibrate reduces significantly at **P**, **T** points higher than **d**. For example, at 22 GPa, 1869 K, equilibration could be achieved in ∼60 ps.

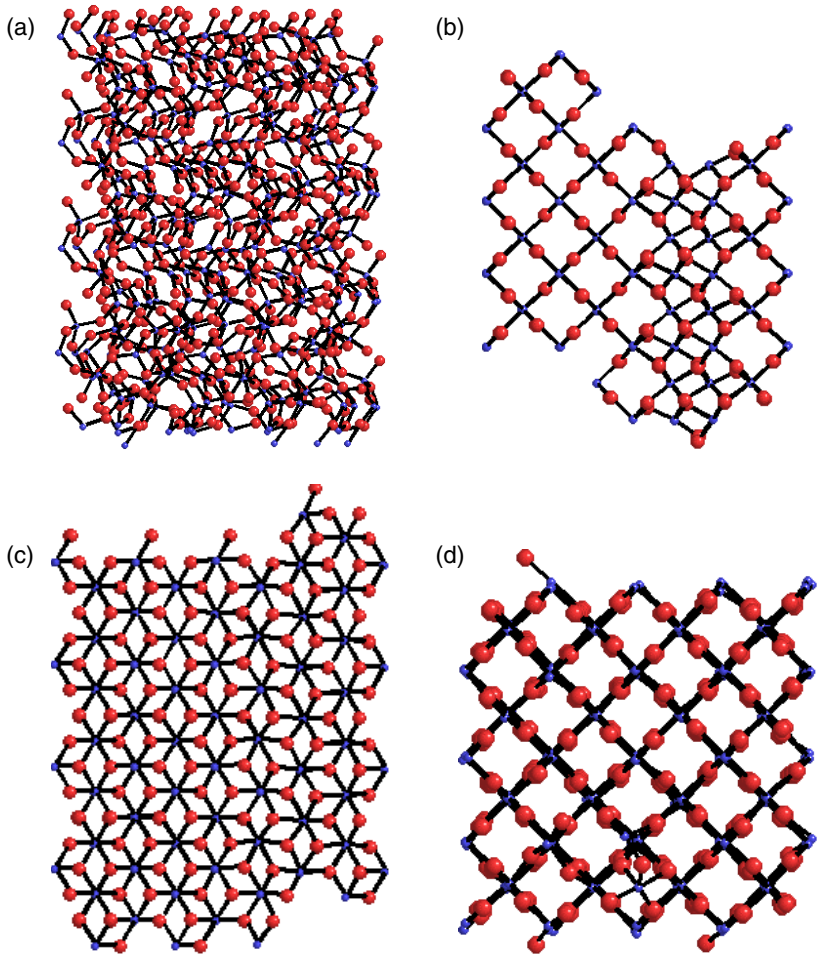

Figure 3. Structures of the new phases at different **P**, **T**, similar to that along the shock Hugoniot: (a) [1 0 0] view at 1410 K, 16.3 GPa, (b) [0 0 1] view at 1682.9 K, 19.9 GPa, (c) [1 0 0] view at 1682.9 K, 19.9 GPa, and (d) [0 0 1] view at 1869.1 K, 22.4 GPa.

The final state at 16.3 GPa, $\mathbf{T} = 1410.1$ K, had a disordered structure despite equilibrating for a very long time as shown in figure 3(a). However, it was observed that on equilibrating the system well beyond 500 ps there was the emergence of a disordered stishovite-like phase. This phase continues to remain disordered on release of pressure and even after annealing at the residual temperatures of 500 and 300 K at $\mathbf{P} = 0.1$ MPa. The diffraction patterns were computed for all these different thermodynamic conditions. It was observed that the disorder at 16.3 GPa, 1410.1 K increased on release of pressure. Once the structure goes into the disordered stishovite phase it is not able to attain the ordered stishovite-like structure even on equilibrating for a long time. Since in shock experiments the sample is subjected to the peak pressure only for a few microseconds, the short duration will further inhibit emergence of an ordered stishovite phase. Therefore, these results may be taken to correspond to the amorphous phase observed in the shock experiments. These simulations also show that on release of pressure and temperature the amorphous phase has 5.2 Si–O coordination.

For thermodynamic conditions beyond **d** (18.1 GPa, 1542.6 K), the equilibrated states display the emergence of the crystalline order. Though all these phases have six Si–O

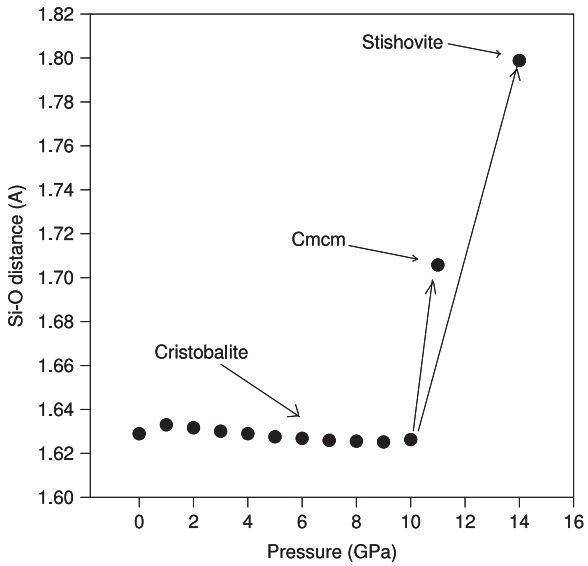

Figure 4. Variation of Si–O distance with pressure under hydrostatic conditions.

coordination, the degree of frozen disorder decreases from **e** to **g** (table 1). Figures 3(b) and (c) show the results of simulations at 19.9 GPa and 1682.9 K. The equilibrated phase when projected on the (100) plane shows almost perfect order. However, when projected on the (001) plane, one can discern the remnants of disorder. The crystalline part of this phase is 'stishovite-like'. At still higher **P** and **T** (22.4 GPa, 1869.1 K) the remaining disorder reduces dramatically, as shown in figure 3(d). Here also the crystalline phase is 'stishovite-like'. Analysis of the evolutionary history of figures 3(b)–(d) shows that α-cristobalite transforms to this stishovite-like phase through an intermediate disordered *Cmcm*-like phase. We shall discuss this issue at more length in section 3.3. In contrast with the calculated behavior of amorphous state at 16.3 GPa, 1410.1 K, the stishovite-like structure at 19.9 GPa became more ordered when annealed at 1200, 1000 and 500 K after release of pressure. Calculated Bragg peaks are found to be the sharpest after annealing at 500 K. These predictions need to be tested by more experiments, as no experimental results are available as to what happens on shock loading to higher pressures.

3.2. Phase transformations under hydrostatic pressures

These simulations were carried out with both sets of pair potentials. Computed **P**–V behavior is similar for both the sets of potentials. However, BKS potentials predict somewhat larger compression along **c**-axis than the results with TTAM potentials. The calculated results when fitted to the Birch–Murnaghan equation [22] gives the bulk modulus $K_o = 25$ GPa (BKS), 26 GPa (TTAM) with $K' = 4$.[7] The volume decreases continuously up to 10 GPa, implying no first order phase transformation up to this pressure. Figure 4 shows the variation of Si–O distance as a function of pressure. A slight increase of $d_{\mathrm{Si-O}}$ observed around 1 GPa has been found to be due to a slight increase in the shear distortion of the cell. Comparison of calculated

[7] When K' is taken equal to 9 as in x-ray diffraction experiments by Downs and Palmer [3] we found that the bulk modulus is 17 GPa, which is comparable to their experimental values of 11 GPa. It is worth mentioning here that the experimental bulk modulus was determined with data only up to pressures of ∼1 GPa as the sample transformed beyond this pressure.

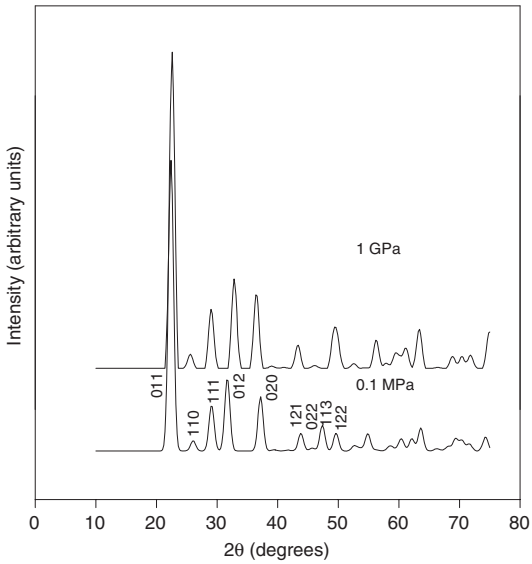

Figure 5. Computed diffraction patterns of cristobalite at ambient pressure and at 1 GPa when compressed at hydrostatic pressures.

diffraction profiles shown in figure 5 also shows some subtle changes in the diffraction pattern. In particular, some diffraction peaks shift to lower 2θ values at higher pressures. Structurally, both these features are due to increase in the shear distortion with respect to the α-structure. However, α-phase does not transform to the monoclinic phase observed in experiments.

We find that under high pressure, the compression of the α-phase is anisotropic and is shown in figure 6 for TTAM potentials. In particular, the compression along the **c**-axis exceeds that along the basal plane. However, the **a**-axis decreases monotonically till 10 GPa, while the **c**-axis flattens off at ∼8 GPa. As the pressure is further increased to ∼10 GPa, the **c**-axis relaxes slightly. This behavior is a precursor to the changes taking place discontinuously at 11 GPa.

In our simulations using the TTAM pair potentials of [10], α-cristobalite transforms to the *Cmcm* phase at ∼11 GPa. However, using the modified pair potentials of Tsuneyuki *et al* [9], this transformation to the *Cmcm* phase takes place at 16 GPa in agreement with the earlier theoretical results. In addition, we also find that if the pressure is increased in much bigger steps (∼5 GPa), the transformation to the *Cmcm* phase is suppressed. The equilibrated *Cmcm* phase as obtained from our simulations at $\mathbf{P} = 11$ GPa is shown in figure 7. It can be clearly seen that it has both four and six Si–O coordination. In the simulations carried out with BKS potentials, *Cmcm* phase does not stabilize and α-cristobalite transforms to stishovite phase at 15 GPa. Therefore, the emergence of *Cmcm* phase depends strongly on the pair potentials, rate of pressure increase and of course on periodic boundary conditions. However, its transformation pressure does not seem to depend upon temperature, as in our simulations α-phase shows no sign of any structural instability up to 1990 K at 10 GPa.

In the α-phase, averaged intra-tetrahedral O–Si–O angles remain almost constant up to 11 GPa. However, increase in the tetrahedral distortion can be seen from increasing differences between various intra-tetrahedral O–Si–O angles as shown in figure 8.[8] In contrast, as shown in figure 9, inter-tetrahedral Si–O–Si angles and Si–Si distances decrease monotonically up

[8] When all the intra-tetrahedral O–Si–O angles in the MD cell are sorted, these fall in four distinct groups. Figure 8 shows the variation of the mean of each group.

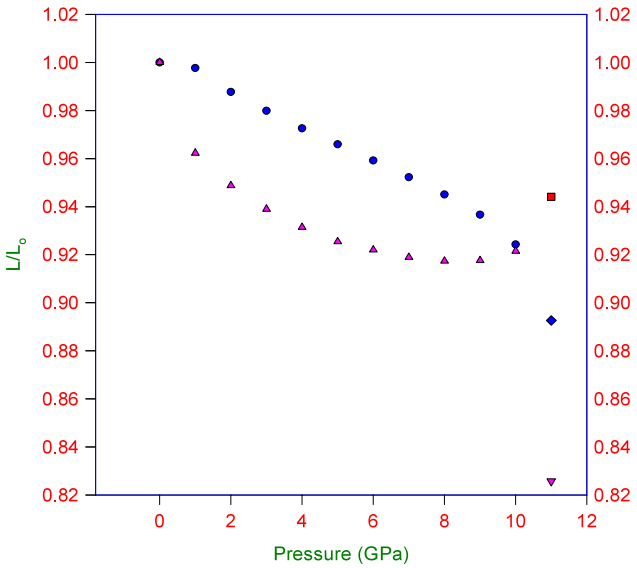

Figure 6. Variation of L/L_0 versus pressure. c/c_0 is shown by ▲ and a/a_0 and b/b_0 of the initial tetragonal phase are shown by ●. However, after the transformation a/a_0, b/b_0 and c/c_0 are shown by ♦, ■ and ▼ respectively.

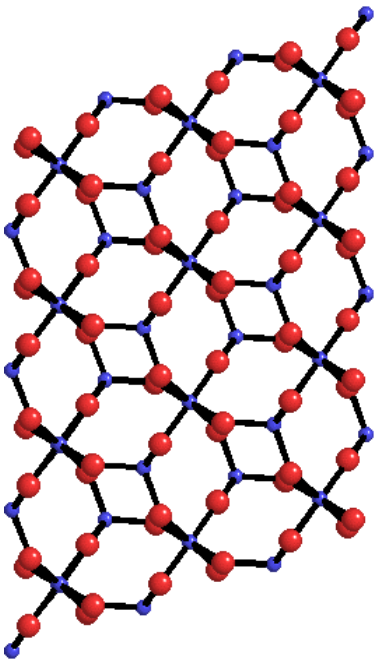

Figure 7. The *Cmcm* phase at 11 GPa using the pair potentials of Tsuneyuki *et al* (only a small section of the central region of the simulated macrocell has been shown).

to 11 GPa for TTAM potentials [10]. This indicates that despite the increase in tetrahedral distortion, the compression of cristobalite is mainly due to the decrease in the inter-tetrahedral distances by bending across the linkage atoms.

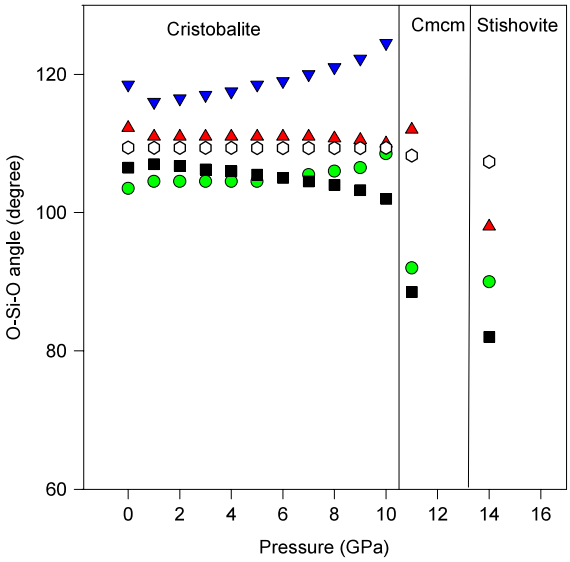

Figure 8. The variation of intra-tetrahedral O–Si–O angles with pressure. The unfilled hexagon shows the mean O–Si–O angle.

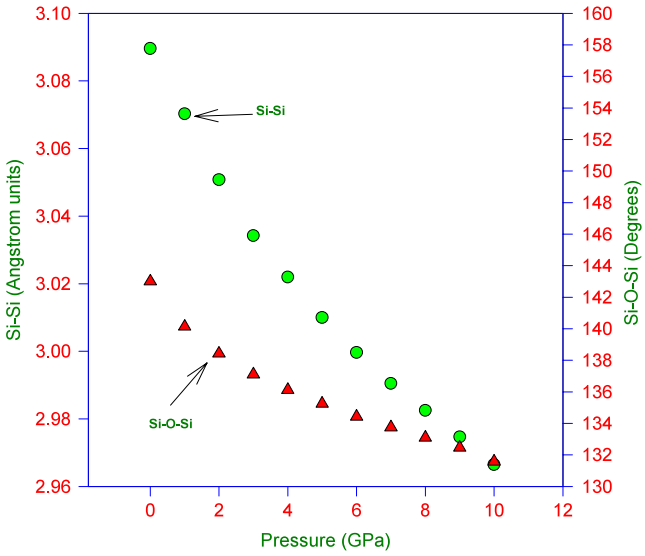

Figure 9. Calculated changes in the inter-tetrahedral Si–O–Si angle and Si–Si distances as a function of pressure.

3.3. Direct transformation to stishovite

We mentioned in the previous section that *Cmcm* phase, which is realized through TTAM potentials, transforms to stishovite at higher pressures. Also, if pressure is raised in somewhat larger steps of 5 GPa, α-phase directly transforms to stishovite. With BKS potentials, α-phase directly transforms to the stishovite phase. These results raise curiosity about the relevance of *Cmcm* phase in the path of transformation from α to stishovite. To understand this, we

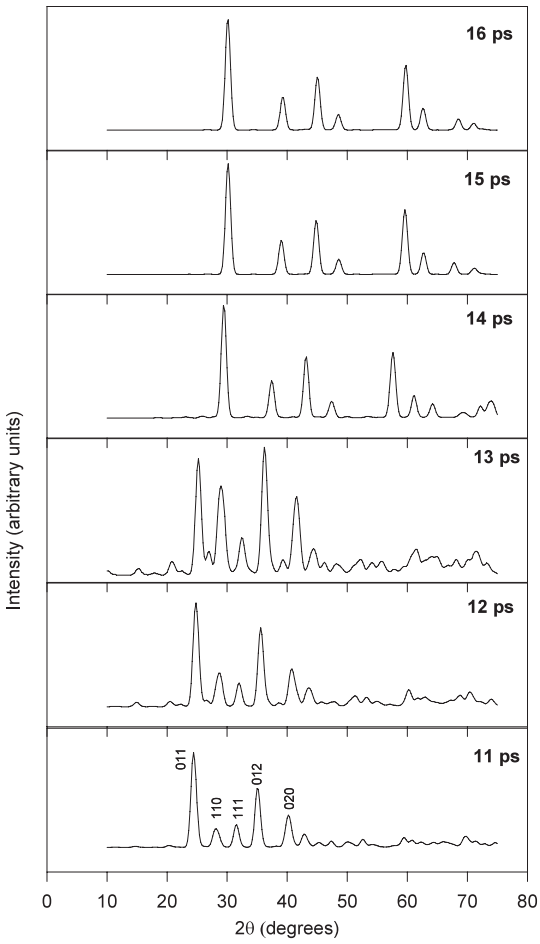

Figure 10. Computed diffraction pattern depicting the transformation from the α-cristobalite to stishovite phase using the BKS potentials.

analyzed the temporal evolution from α to stishovite phase when simulations were carried out with the BKS potentials. We find that the α-phase continues to persist till 10 ps at 15 GPa, and then within next 5 ps the transformation is complete. Our results display that α- transforms to stishovite phase through an intermediate *Cmcm*-like phase. In this context, the only difference between TTAM and BKS pair potentials is that with the former potentials *Cmcm* phase has a range of stability.

Calculated diffraction shown in figure 10 confirms that at 11 ps the structure is α-phase, at 13 ps it is similar to *Cmcm* phase and at 15 ps it is that of stishovite phase. Figure 11 shows the structural evolution from α-phase to stishovite as predicted in our simulations with the BKS potentials. One can clearly discern a bond making between **S1** (silicon) and **O5** (oxygen) and bond breaking between **S1** and **O2** at 12 ps. At 14 ps **O2** and **O6** coordinate to **S1** and structure then relaxes to almost perfect order by 15 ps. At 13 ps structure is almost *Cmcm*. These results show that no diffusion is necessary to bring about a transformation from α-cristobalite to stishovite phase through the *Cmcm* phase. A slight local atomic rearrangement is all that is needed to cause the structural change.

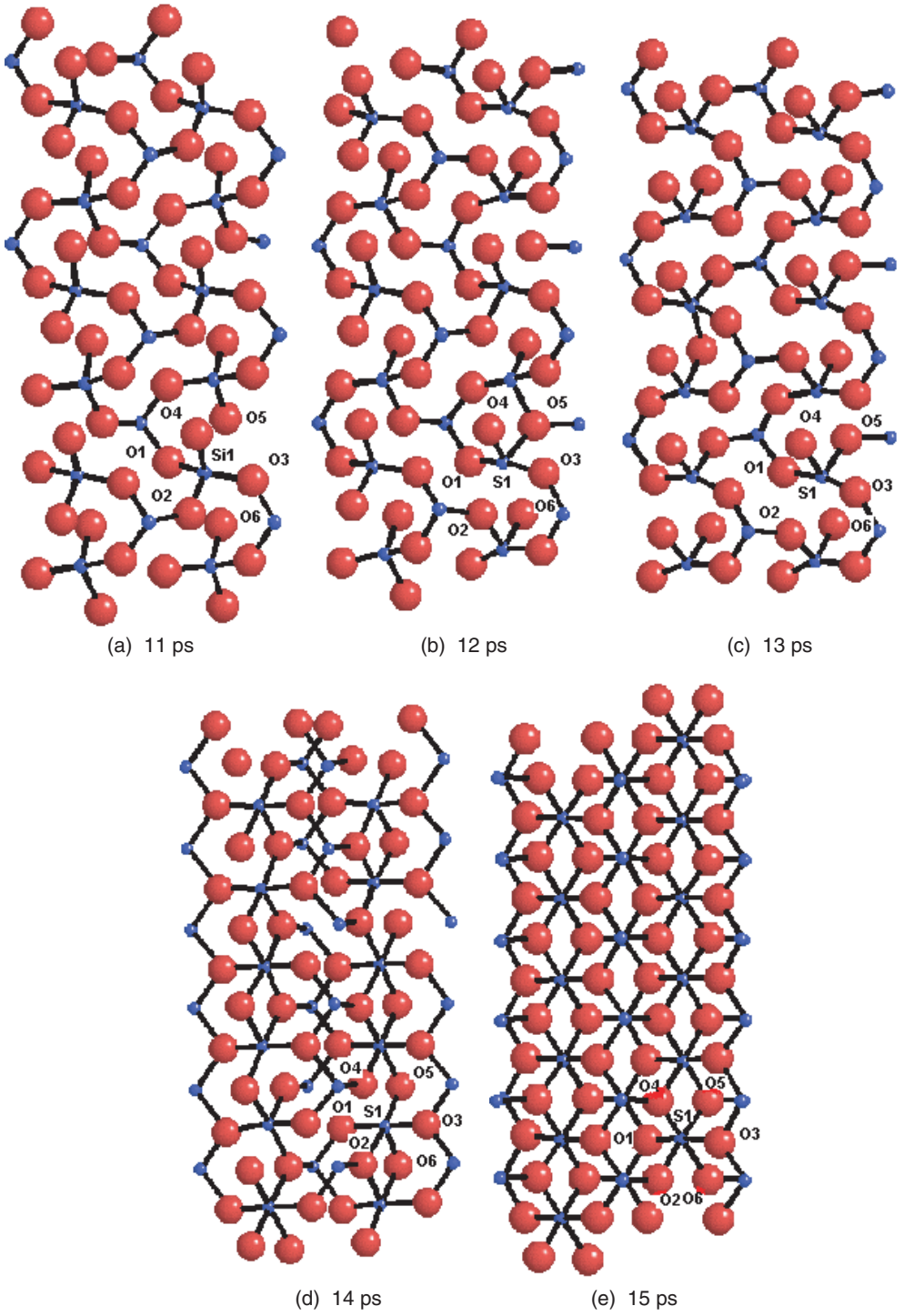

Figure 11. Temporal evolution of the stishovite phase.

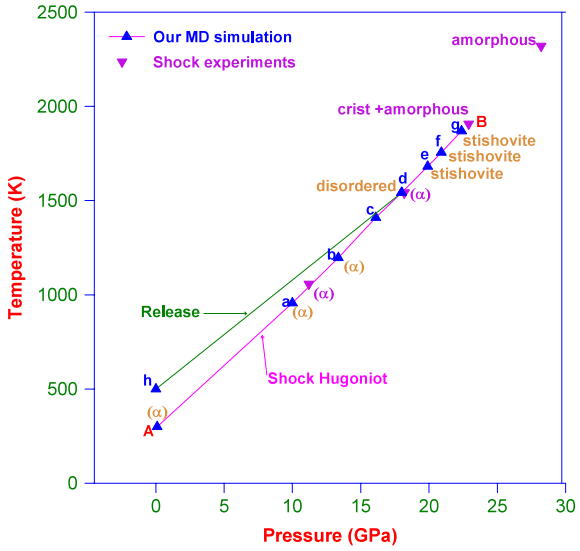

Figure 12. Summary of simulations carried out at pressures and temperatures representative of shock experiments of Gratz *et al* [1].

It is interesting to find out what triggers the observed coordination change. In general, under compression, the non-bonded atoms cannot be brought closer than some limiting value without an excessive cost in terms of energy. When the energy of compression of these distances becomes comparable to the cohesive energy differences between the structures, the initial structure becomes unstable. A survey of a large number of materials indicates that the extreme limiting value of O···O is ∼2.62 Å [23]. It is interesting to note that just before the transition the sites at which the transformation is initiated are those where the non-bonded O···O distance was ∼2.42 Å, i.e. lower than the extreme limiting distance. Therefore, our simulations show that the nucleation for the phase transformation starts at the sites where the O···O distances are highly constrained.

4. Conclusions

To conclude, we present the summary of our simulations in figure 12. Our simulations show a transformation to a disordered phase beyond 16 GPa and to a 'stishovite-like' phase beyond 18 GPa. As in all simulations, the differences in the observed and calculated pressures of transformations depend on the pair potentials. In addition, these differences may also arise from the differences in the rate and nature of increase of pressure and temperature as compared to the experiments. Emergence of an ordered phase at higher pressures should encourage more experiments on shock loading of cristobalite. Our simulations under static pressures show that stishovite phase emerges through *Cmcm* phase. In addition, if the pressure is raised in larger steps, the *Cmcm* phase is bypassed and alpha cristobalite transforms directly to a stishovite-like phase. Since the *ab initio* calculations of Klug *et al* were carried out in steps of 10 GPa, it is possible that the *Cmcm* phase was bypassed, resulting in direct transformation to the stishovite phase [16].

References

[1] Gratz A J, DeLoach L D, Clough T M and Nellis W J 1993 *Science* **259** 663
[2] Palmer D C and Finger L W 1994 *Am. Miner.* **79** 1

[3] Downs R T and Palmer D C 1994 *Am. Miner.* **79** 9
[4] Yamakata M and Yagi T 1996 *Technical Report* ISSP University of Tokyo
[5] Tsuchida Y and Yagi T 1990 *Nature* **347** 267
[6] Palmer D C, Hemley R J and Prewitt C T 1994 *Phys. Chem. Miner.* **21** 481
[7] Onodera A, Suito K, Namba J, Taniguchi Y, Horikawa T, Miyoshi M, Shimomura O and Kikegawa T 1997 *High Pressure Res.* **15** 307
[8] Parise J B, Yeganeh-Haeri A and Weidner D J 1994 *J. Appl. Phys.* **75** 1361
[9] Tsuneyuki S, Matsui Y, Aoki H and Tsukada T 1989 *Nature* **339** 209
[10] Tsuneyuki S, Tsukada M, Aoki H and Matsui Y 1988 *Phys. Rev. Lett.* **61** 869
[11] Tse J S and Klug D D 1991 *J. Chem. Phys.* **95** 9176
[12] Keskar N R and Chelikowsky J R 1992 *Phys. Rev.* B **46** 1
[13] Dove M, Tucker M, Redfern S, Craig M, Trachenko K, Marshall W and Keen D *ISIS Annual Report 1999–2000* p 32
[14] Boisen M B Jr and Gibbs G V 1993 *Phys. Chem. Miner.* **20** 123
[15] van Beest B W H, Kramer G J and van Santen R A 1990 *Phys. Rev. Lett.* **64** 1955
[16] Klug D D, Rousseau R, Uehara K, Bernasconi M, Le Page Y and Tse J S 2001 *Phys. Rev.* B **63** 104106
[17] Melchionna S, Ciccotti G and Holian B L 1993 *Mol. Phys.* **78** 533
[18] Hoover W G 1985 *Phys. Rev.* A **31** 1695
[19] Smith W and Forester T R 1996 Copyright Council for Central Laboratory of Research Councils, Daresbury Laboratory at Daresbury, Nr. Warrington
[20] Heany P J 1994 *SILICA* ed P J Heany, C T Prewitt and G V Gibbs (Washington, DC: Miner. Soc. America) p 1
[21] Kadau K, Germann T C, Lomdahl P S, Albers R C, Wark J S, Higginbotham A and Holian B L 2007 *Phys. Rev. Lett.* **98** 135701
[22] Birch F 1978 *J. Geophys. Res.* **83** 1257
[23] Sharma S M and Sikka S K 1996 *Prog. Mater. Sci.* **40** 1–77